DOI: 10.1002/ejic.200901206

# Synthesis, Structure, and Magnetic Properties of Amine-Templated Transition-Metal Phosphites

**Padmini Ramaswamy,[a] Sukhendu Mandal,[a] Nayana N Hegde,[a] Ramanath Prabhu,[a] Debmalya Banerjee,[b] S. V. Bhat,[b] and Srinivasan Natarajan*[a]**

**Keywords:** Solvothermal synthesis / X-ray diffraction / Transition metals / Phosphorus / Open frameworks

Transition-metal phosphites of cobalt and vanadium, $[C_4N_2H_{12}][Co(HPO_3)_2]$ (**I**), $[C_4N_2H_{14}][Co(HPO_3)_2]$ (**II**), $[Co(C_{10}H_8N_2)(H_2PO_3)_2]$ (**III**), $[C_4N_2H_{14}][V^{III}F(HPO_3)_2]\cdot H_2O$ (**IV**), and $[C_3N_2H_5]_2[V_4^{III}(H_2O)_3(HPO_3)_4(HPO_4)_3]$ (**V**), have been synthesized and characterized. Organophosphorus esters were employed to stabilize cobalt in tetrahedral coordination and also to prepare the low-dimensional structures, which are otherwise difficult to synthesize. The structures have one- (**I**, **II**, **IV**), two- (**III**) and three-dimensionally (**V**) extended networks built up by the linking of metal polyhedra and phosphite units. Another vanadyl phosphite, $[C_2N_2H_{10}][(V^{IV}O)_3(H_2O)(HPO_3)_4]\cdot H_2O$,[15] was also prepared and investigated extensively by ESR, magnetic susceptibility, and other studies. All the compounds in the present study exhibit antiferromagnetic interactions. Well-established magnetic models have been used to fit the experimental data. The compounds have also been characterized in detail by using UV/Vis spectroscopic studies.

## Introduction

Compounds possessing channels and cavities have much potential to be utilized in the areas of catalysis, sorption, and other related processes.[1–3] Though the aluminosilicate zeolites are the most widely studied class of compounds that exploit open spaces,[2,3] the discovery of aluminophosphates with comparable structures in the early 1980s[4] are equally important. The aluminophosphates, prepared by employing a variety of organic amines, provided the necessary impetus to investigate phosphate structures of other metals. This resulted in a large variety of phosphate framework structures that now incorporate most of the elements of the periodic table.[1,3]

During the course of these studies, it has also been established that other related anions such as the arsenates, phosphites, selenites, selenates, sulfites, and sulfates can also be incorporated as part of the family of extended network structures.[1–3,5] Each one of these anions is important from a structural point of view, as they provide diversity that depends on the charge, size, shape, and the number of binding sites. Of these, the phosphite structures appear to resemble the phosphate analogues, as has been shown in the family of zinc phosphites.[6]

Transition-metal phosphites have also been prepared and characterized over the years.[7] The transition elements provide opportunities to investigate the interplay of coordination preferences, oxidation states, and ligand geometries and to correlate them with well-founded theoretical models available in the literature.[1,5] The earliest study of transition-metal phosphites was carried out by Zubeita and co-workers, who isolated a 3D vanadium phosphite, $[H_2N(CH_2CH_2)_2NH_2][(V^{IV}O)_3(HPO_3)_4(H_2O)_2]$.[7a] The directional synergy between the framework and the organic amine was established by Harrison in $[CN_3H_6]_2[(V^{IV}O)_3(H_2O)_3(HPO_3)_4]\cdot 3H_2O$.[8] Rojo and co-workers reported new phosphite structures of cobalt.[7f,9]

We have been interested in the study of phosphite-based compounds for some time and have discovered interesting frameworks.[1,10] In continuation of this theme, we have now isolated five new amine-templated open-framework phosphite structures based on vanadium and cobalt. The compounds, $[C_4N_2H_{12}][Co(HPO_3)_2]$ (**I**), $[C_4N_2H_{14}][Co(HPO_3)_2]$ (**II**), $[Co(C_{10}H_8N_2)(H_2PO_3)_2]$ (**III**), $[C_4N_2H_{14}][V^{III}F(HPO_3)_2]\cdot H_2O$ (**IV**), and $[C_3N_2H_5]_2[V_4^{III}(H_2O)_3(HPO_3)_4(HPO_4)_3]$ (**V**), have been prepared by solvothermal methods and their structures were determined by using single-crystal X-ray diffraction. In this paper, we present the synthesis, structure, and characterization of these compounds.

[a] Framework solids Laboratory, Solid State and Structural Chemistry Unit, Indian Institute of Science, Bangalore 560012, India
Fax: +91-80-2360-1310
E-mail: snatarajan@sscu.iisc.ernet.in
[b] Department of Physics, Indian Institute of Science, Bangalore 560012, India

Supporting information for this article is available on the WWW under http://dx.doi.org/10.1002/ejic.200901206.

  

## Results and Discussion

### Cobalt Phosphite Structures

#### *Structure of $[C_4N_2H_{12}][Co(HPO_3)_2]$ (I) and $[C_4N_2H_{14}][Co(HPO_3)_2]$ (II)*

The asymmetric units of **I** and **II** consist of eight non-hydrogen atoms. The Co atom is tetrahedrally coordinated to four oxygen atoms in both structures, which is consistent with the deep-blue color of the compounds. The average Co–O bond length is 1.955 Å for **I** and 1.951 Å for **II**. The cobalt atoms are connected to the phosphorus atoms through four Co–O–P linkages with an average angle of 135.75° for **I** and 132.70° for **II**. The phosphorus atoms in both structures are connected to the cobalt atoms through two Co–O–P linkages and possess one terminal P–O bond. Selected bond lengths are listed in Table S1 (Supporting Information).

The structures of **I** and **II** have the same building units. Thus, the $CoO_4$ and $HPO_3$ units are strictly alternating and they are connected through their vertices to form four-membered rings, which are further linked through their corners, giving rise to 1D anionic $[Co(HPO_3)]^{2-}$ chains. Diprotonated piperazine (in **I**) and 1,4-diaminobutane molecules (in **II**) act as the charge-compensating cations and occupy the interchain spaces, which interact with the cobalt phosphite units through C–H···O and N–H···O hydrogen bonds (Figures 1a and 2a). These interactions give rise to supramolecularly arranged 2D layers. The observed hydrogen-bond interactions are listed in Table 1. The projection of the structures down the chain axis, showing the layout of the adjacent chains is given in Figures 1b and 2b, respectively.

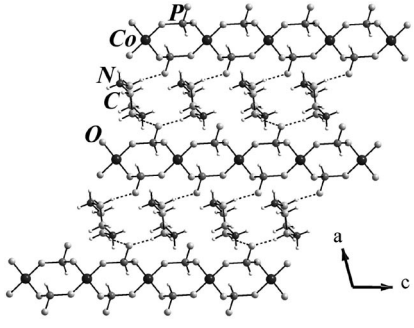


(a)

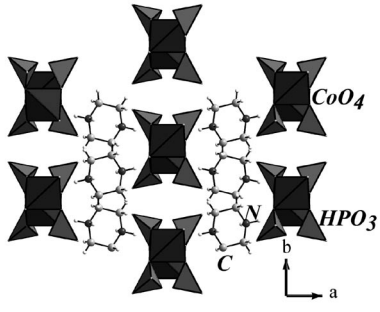


(b)

Figure 1. (a) The 1D cobalt phosphite chains and the organic amine molecules in $[C_4N_2H_{12}][Co(HPO_3)_2]$ (**I**). Dotted lines represent the possible hydrogen bond interactions. (b) View of the arrangement of the chains down the chain axis. Note that each of the chains is surrounded by six other ones.

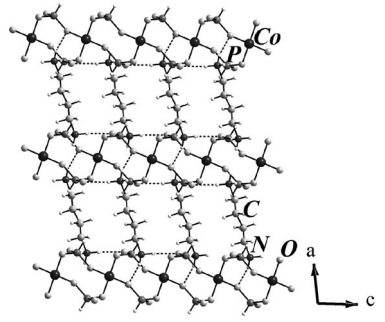


(a)

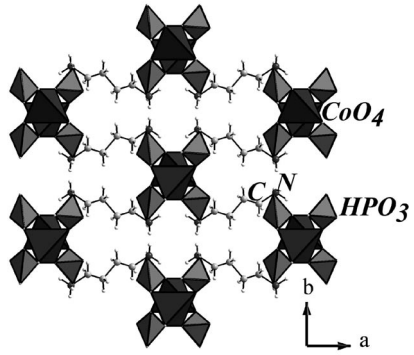


(b)

Figure 2. (a) The 1D cobalt phosphite chains and the organic amine molecules in $[C_4N_2H_{14}][Co(HPO_3)_2]$ (**II**). Dotted lines represent the possible hydrogen bond interactions. (b) View of the arrangement of the chains down the chain axis. Note that each of the chains is surrounded by six other ones.

Table 1. Important observed hydrogen-bond interactions in compounds **I**–**III**.

| D–H···A | D–H [Å] | H···A [Å] | D···A [Å] | D–H···A [°] |
|---|---|---|---|---|
| Compound **I** | | | | |
| C(1)–H(1A)···O(3) | 0.97 | 1.75 | 2.708(4) | 170 |
| C(1)–H(1B)···O(3) | 0.97 | 1.75 | 2.682(5) | 161 |
| Compound **II** | | | | |
| N(1)–H(1A)···O(2) | 0.89 | 2.02 | 2.890(5) | 164 |
| N(1)–H(1B)···O(3) | 0.89 | 1.93 | 2.769(5) | 157 |
| N(1)–H(1C)···O(3) | 0.89 | 1.86 | 2.737(5) | 168 |
| Compound **III** | | | | |
| C(2)–H(4)···O(5) | 0.93 | 2.52 | 3.432(6) | 167 |
| C(5)–H(6)···O(4)[a] | 0.93 | 2.40 | 3.303(6) | 163 |
| C(7)–H(8)···O(4) | 0.93 | 2.42 | 3.242(6) | 147 |

[a] *Intra*.

  

### *Structure of [Co($C_{10}H_8N_2$)($H_2PO_3$)$_2$] (III)*

The asymmetric unit of **III** consists of 21 non-hydrogen atoms. The Co atom in **III** is octahedrally coordinated to four oxygen and two nitrogen atoms, with an average Co–O/N bond length of 2.146 Å. Each cobalt atom is connected to two distinct phosphorus atoms through four Co–O–P linkages, with an average angle of 131.7°. Of the two phosphorus atoms, P(1) is connected to the cobalt atom through one Co–O–P linkage and possesses two terminal P–O bonds, whereas P(2) has two Co–O–P linkages and possesses one P–O terminal bond. Bond valence sum calculations[11] and bond length considerations indicate that P(1)–O(5) with a distance of 1.553(3) Å and P(2)–O(6) with a distance of 1.556(3) Å are protonated. This was further supported by the observation of a proton position next to the oxygen atoms in the difference Fourier maps. Thus, both the phosphite units are $H_2PO_3$ groups. Selected bond lengths are listed in Table S1 (Supporting Information).

In compound **III**, $CoO_4N_2$ octahedra are connected together to form $Co_2O_6N_4$ dimeric units. The dimers are further connected through $H_2P(2)O_3$ units to form a 1D chain (Figure 3a). $H_2P(1)O_3$ units are connected to these chains through the three-coordinate oxygen atom, O(3), and hang freely. The 1D chains are further connected by 4,4′-bipyridine ligands to form a 2D layer structure (Figure 3b). The observation of a free hanging phosphite unit has been made for the first time in transition-metal phosphite structures.

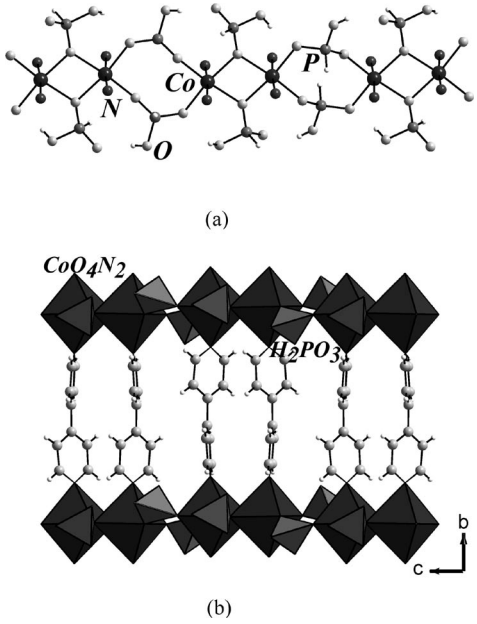


Figure 3. (a) The inorganic chains in [Co($C_{10}H_8N_2$)($H_2PO_3$)$_2$] (**III**). Note the formation of the $CoO_4N_2$ dimers and their connectivity through $H_2PO_3$ units. (b) The connectivity between the chains through the 4,4′-bipyridine ligands.

## Vanadium Phosphite Structures

### *Structure of [$C_4N_2H_{14}$][$V^{III}F(HPO_3)_2$]·$H_2O$ (IV)*

The asymmetric unit of **IV** contains nine non-hydrogen atoms. The vanadium and phosphorus atoms occupy special positions with site multiplicities of 0.25 (4d) and 0.50 (8 h), respectively. The vanadium atom is octahedrally coordinated with four oxygen and two fluorine atoms with an average V–O/F distance of 1.967 Å. The vanadium atom forms four V–O–P linkages and two V–F–V linkages (av. 135.9°). The phosphorus atom makes two V–O–P linkages and possesses one P=O terminal bond. Selected bond lengths are listed in Table S1 (Supporting Information).

In the structure of **IV**, vanadium atoms are connected through the *trans* positioned fluorine atoms to form a 1D –V–F–V– chain. The $HPO_3$ units are grafted onto this chain such that each vanadium octahedron shares four oxygen atoms with four distinct $HPO_3$ units, giving rise to a 1D chain, $[VF(HPO_3)_2]^{2-}$ (Figure 4a; Figure S1, Supporting Information). The structure closely resembles the mineral *tancoite*, $LiNaHAl(PO_4)_2(OH)_2$.[12] The individual chains are spatially arranged to form a hexagon (Figure 4b) and similar arrangements have been observed before in many phosphate structures.[1]

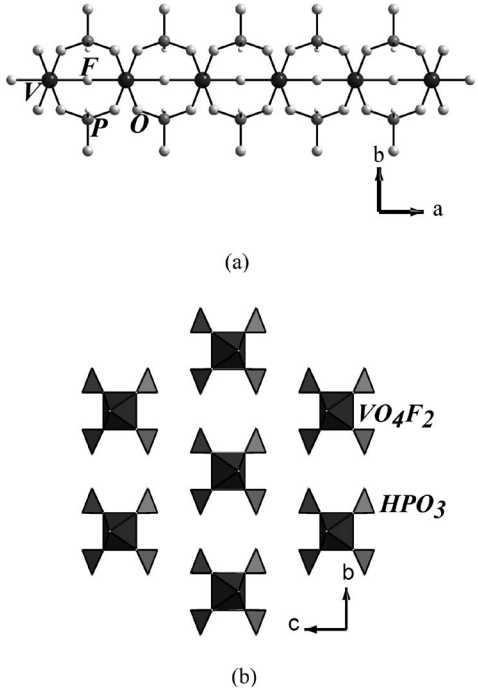


Figure 4. (a) The inorganic chain structure in [$C_4N_2H_{14}$][$V^{III}F(HPO_3)_2$]·$H_2O$ (**IV**). (b) View of the arrangement of the chains down the chain axis. Note that each of the chains is surrounded by six other ones.

### *Structure of [$C_3N_2H_5$]$_2$[$V_4^{III}(H_2O)_3(HPO_3)_4(HPO_4)_3$] (V)*

The asymmetric unit of **V** consists of 18 non-hydrogen atoms. Of these, two vanadium atoms, V(1) [2b], V(2) [2a], and one phosphorus atom, P(3) [4d], occupy special positions with site multiplicities of 0.16 for V(1) and V(2) and 0.33 for P(3). All the vanadium atoms are octahedrally coordinated with six oxygen atom neighbors with an average V–O bond length of 2.012 Å for V(1), 2.003 Å for V(2), and 2.001 Å for V(3). The V(1) and V(2) atoms form six V–O–

  

P linkages [av. 139.2° for V(1), 131.5° for V(2)], and V(3) makes five V–O–P linkages (av. 139.8°) and possesses one terminal V–$OH_2$ bond. All three phosphorus atoms make three V–O–P linkages. Whereas P(1) and P(3) belong to $HPO_3$ groups, P(2) belongs to a $HPO_4$ group. Thus, both phosphite and phosphate groups exist in this structure. Because the starting mixture does not contain any phosphoric acid, the phosphate group must have formed by the oxidation of the phosphite species during the synthesis. Similar formation of phosphate species from the phosphite has been observed before.[10a] Selected bond lengths are listed in Table S1 (Supporting Information).

The 3D structure of **V** can be understood by considering two different connectivities involving the vanadium octahedra and the phosphite and the phosphate units. Thus, the $V(3)O_5(H_2O)$ and $HP(2)O_4$ units are connected through their vertices to form six-membered rings, which are capped by $HP(3)O_3$ moieties. The capped six-membered units are connected together to form a cationic layer of the formula $[V_3(H_2O)_3(HPO_4)_3(HPO_3)]^+$, encompassing circular 12-membered rings (Figure 5a). The layers are topologically similar to that observed in many layered amine-templated aluminophosphates.[13] The layers are arranged one over the other in an *AAA*··· fashion and are connected by anionic 1D vanadium phosphite chains, $[V(HPO_3)_3]^{3-}$ (Figure 5b). The 1D chains, formed by the connectivity involving V(1) $O_6$, $V(2)O_6$ and $HP(1)O_3$ units, penetrate the vanadium phosphite–phosphate layers perpendicularly. This connectivity gives rise to a pillared layer arrangement where the pillars pass through the 12-membered apertures within the layers (Figure 6; Figure S2, Supporting Information). This arrangement gives rise to interconnected channels bound by 14 T atoms (T = V, P). The disordered amine molecules and imidazolium cations occupy the 14-membered channels. Similar pillared-layer structures have been observed in the indium phosphate $In_9(HPO_4)_{14}(H_2O)_6F_3\cdot(C_{10}N_2H_9)_3\cdot(H_3O)\cdot(H_2O)_2$[14a] and in the vanadium phosphite $(C_4H_8N_2H_4)_{0.5}$-$(C_4H_8N_2H_3)[V_4(HPO_3)_7(H_2O)_3]1.5H_2O$.[14b]

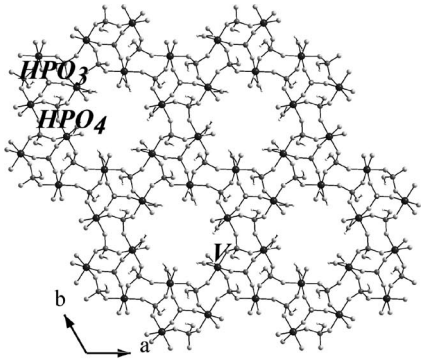


(a)

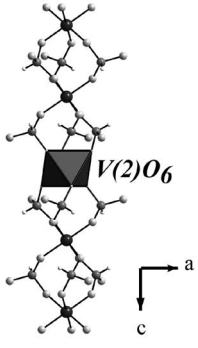


(b)

Figure 5. (a) The inorganic layer in $[C_3N_2H_5]_2[V_4^{III}(H_2O)_3$-$(HPO_3)_4(HPO_4)_3]$ (**V**). Note the 12-membered aperture in the middle. (b) The 1D chain $[V(HPO_3)_3]^{3-}$ that connects the layers in **V**.

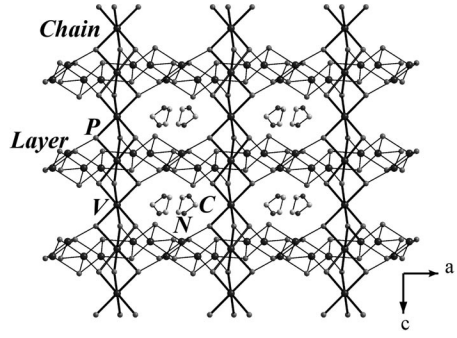


Figure 6. The T atom connectivity shows the linkage between the layers through the 1D chains in **V**. The 14-membered channels are occupied by imidazole cations (see text).

### *$[C_2N_2H_{10}][(V^{IV}O)_3(H_2O)(HPO_3)_4]\cdot H_2O$ (VI)*

During the course of the present investigation, we also succeeded in preparing a compound with vanadium in the +4 oxidation state, $[C_2N_2H_{10}][(V^{IV}O)_3(H_2O)(HPO_3)_4]\cdot H_2O$. The synthesis and structural studies of this compound have been previously established by Feng et al.[15] (Figure S3, Supporting Information). As part of this study, we have carried out detailed magnetic and electron spin resonance (ESR) investigations on this compound.

## Discussion

As part of a study on transition-metal phosphites, three cobalt phosphites (**I**–**III**) and two vanadium phosphites (**IV** and **V**) have been prepared and characterized. For the preparation of the low-dimensional phases of cobalt, **I** and **II**, we employed triethylphosphite (TEP) as the phosphorus source. The use of tributyl phosphate as the source of phosphorus for the synthesis of new phosphate phases of zinc,[16a] cobalt,[16a,16b] and manganese[16c] with novel structural features has been known. It has been postulated that the slow hydrolysis of the phosphate ester may be responsible for the observation of new types of structures in these compounds. Similarly, the use of triethylphosphite possibly enables a controlled release of the phosphite ions in solution and could have provided some kinetic control in the formation of the 1D cobalt phosphite phases. It may be noted that the formation of low-dimensional structures of cobalt, especially in tetrahedral coordination, is always dif-

  

ficult and novel approaches may be required to stabilize such phases. 1D cobalt phosphates with $Co^{2+}$ ions in tetrahedral coordination have been stabilized by the use of amine phosphates.[17] In the present study, the use of organic esters could be responsible for the stabilization of tetrahedral cobalt as well as the low-dimensional structures in cobalt phosphites **I** and **II**. A new type of 1D chain structure is connected through the 4,4′-bipyridine units, forming the layer in **III**. The synthesis of this phase was facilitated by employing normal hydrothermal methods, which incidentally stabilized the octahedral cobalt species unlike in **I** and **II**, where tetrahedral cobalt is present. This observation also suggests the importance of the reaction conditions during the preparation of framework compounds containing cobalt.

Compounds **IV** and **V** have vanadium in the +3 oxidation state and both structures bear a close resemblance to the other phosphite and phosphate compounds reported in the literature.[1] Thus, $[C_4N_2H_{14}][V^{III}F(HPO_3)_2]\cdot H_2O$ (**IV**) closely resembles the mineral tancoite, $LiNaHAl(PO_4)_2(OH)_2$.[18] Though transition-metal phosphates with tancoite chain structures are known, this is the first report of a tancoite structure among the transition-metal phosphites. Compound **V**, $[C_3N_2H_5]_2[V_4^{III}(H_2O)_3(HPO_3)_4(HPO_4)_3]$, has a close structural relationship with many structures reported in the literature.[13,14] The closest relationship has been observed with the iron phosphite $[C_4N_2H_{12}][Fe^{III}_4(H_2O)_3(HPO_3)_7]\cdot(H_2O)_x$, $x = 0.6$, reported by us.[10b]

The stability of compound **I** was observed to be not very good when exposed to atmospheric conditions, and we could not characterize this phase satisfactorily. We have, however, characterized all other compounds by using UV/Vis spectroscopic and magnetic studies. The previously known vanadium phosphite $[C_2N_2H_{10}][(V^{IV}O)_3(H_2O)(HPO_3)_4]\cdot H_2O$ (**VI**) was also studied in detail.

## UV/Vis Spectroscopic Studies

UV/Vis absorption spectra were recorded in the solid state (Perkin–Elmer, lambda 35) at room temperature, which indicates the presence of $Co^{II}$ in tetrahedral and octahedral coordination environments in compounds **II** and **III**, respectively, $V^{III}$ in compounds **IV**, **V**, and $V^{IV}$ in compound **VI** (Table 2; Figure S4, Supporting Information). The diffuse reflectance spectrum of $[C_4N_2H_{14}][Co(HPO_3)_2]$ (**II**) shows bands at 18181, 17159, and 15734 $cm^{-1}$, which can be assigned to the $\nu_3$ transition $[^4T_1(P)\leftarrow{}^4A_2]$ (generally appears as multiple transitions). The $\nu_2$ band $[^4T_1(F)\leftarrow{}^4A_2]$ generally appears in the near-infrared region, which was not observed. We also observed a shoulder at ca. 24096 $cm^{-1}$, which indicates the possible presence of a small amount of $Co^{3+}$ ions in octahedral coordination ($^1A_{1g}\rightarrow{}^1T_{2g}$). Similar observations have also been made earlier in compounds containing tetrahedral cobalt.[19a] In the case of $[Co(C_{10}H_8N_2)(H_2PO_3)_2]$ (**III**), the absorption band at 30760 $cm^{-1}$ can be assigned to the intraligand π–π* transition of the bpy unit. Compound **III** exhibits a redshifted absorption relative to the ligand, which may be due to the perturbation of the π–π* transition of the free bpy unit on bonding with the metal atom. Similar absorption shifts of the bonded bpy units have been observed before.[19b,19c] The bands at 19287 and 8560 $cm^{-1}$ can be assigned to the transitions from the $^4T_{1g}$ ($^4F$) fundamental state to the excited levels $^4T_{1g}(^4P)$ and $^4T_{2g}(^4F)$, respectively, whereas a shoulder at 16236 $cm^{-1}$ corresponds to a weak transition to the excited level $^4A_{2g}(^4F)$. We have made estimates of the $D_q$ and Racah parameter $B$ values by fitting the observed absorption frequencies to the energy expressions for a $d^7$ ion.[20] The calculated values of $D_q$ and $B$ are 738 and 657 $cm^{-1}$, respectively. The reduction of the $B$ parameter value with respect to that of the free ion (1115 $cm^{-1}$)[20] sug-

Table 2. The observed UV/Vis bands and the corresponding transitions for compounds **II**–**V**.

| Compound | Frequency [$cm^{-1}$] | Assignment | Symmetry |
|---|---|---|---|
| **II** | 18181, 17159 15734 | $^4T_1(P) \leftarrow {}^4A_2$ | $Co^{2+}$ ($T_d$) |
| | 24096 (sh.) | $^1A_{1g} \rightarrow {}^1T_{2g}$ | $Co^{3+}$ ($O_h$) |
| **III** | 30760 | intraligand π–π* transition of bpy | |
| | 19287 | $^4T_{1g}(^4P) \leftarrow {}^4T_{1g}(^4F)$ | $Co^{2+}$ ($O_h$) |
| | 16236 (sh.) | $^4A_{2g}(^4F) \leftarrow {}^4T_{1g}(^4F)$ | |
| | 8560 | $^4T_{2g}(^4F) \leftarrow {}^4T_{1g}(^4F)$ | |
| **IV** | 14685 | $^3T_{2g}(^3F) \leftarrow {}^3T_{1g}(^3F)$ | |
| | 22896 | $^3T_{1g}(^3P) \leftarrow {}^3T_{1g}(^3F)$ | $V^{3+}$ ($O_h$) |
| | 29878 | $^3A_{2g}(^3F) \leftarrow {}^3T_{1g}(^3F)$ | |
| | 11389 (sh.) | spin forbidden $^1E_g(^1D)$ $^1T_{2g}(^1D) \leftarrow {}^3T_{1g}$ | |
| **V** | 14814 | $^3T_{2g}(^3F) \leftarrow {}^3T_{1g}(^3F)$ | |
| | 22675 | $^3T_{1g}(^3P) \leftarrow {}^3T_{1g}(^3F)$ | $V^{3+}$ ($O_h$) |
| | 29498 | $^3A_{2g}(^3F) \leftarrow {}^3T_{1g}(^3F)$ | |
| | 11037 (sh.) | spin forbidden $^1E_g(^1D)$, $^1T_{2g}(^1D) \leftarrow {}^3T_{1g}$ | |
| $[C_2N_2H_{10}][(V^{IV}O)_3(H_2O)(HPO_3)_4]\cdot H_2O$[15] | 11037 | $^2B_2 \leftarrow {}^2E$ | |
| | 15313 | $^2B_2 \leftarrow {}^2B_1$ | $VO^{2+}$ |
| | 22321 | $^2B_2 \leftarrow {}^2A_1$ | |

  

gests that the Co–O/N bonds are significantly covalent. Similar values of $D_q$ and $B$ have been observed in other amine-containing open-framework cobalt phosphite compounds.[7f,9] The vanadium phosphite compounds $[C_4N_2H_{14}][V^{III}F(HPO_3)_2]\cdot H_2O$ (**IV**) and $[C_3N_2H_5]_2[V_4^{III}(H_2O)_3(HPO_3)_4(HPO_4)_3]$ (**V**) show the spin-allowed transitions from the fundamental state $^3T_{1g}(^3F)$ to the excited levels $^3T_{2g}(^3F)$, $^3T_{1g}(^3P)$, and $^3A_{2g}(^3F)$ at frequencies of 14685, 22896, and 29878 $cm^{-1}$ for **IV** and 14814, 22675, and 29498 $cm^{-1}$ for **V**. The spin-forbidden transition $^3T_{1g}(^3F)\rightarrow{}^1E_g(^1D)$, $^1T_{2g}(^1D)$ was observed as a shoulder on the first band at 11389 (**IV**) and 11037 $cm^{-1}$ (**V**). The calculated $D_q$ and Racah parameter $B$ values for the $V^{III}$ ($d^2$) ion are $D_q$ = 1519 $cm^{-1}$, $B$ = 581 $cm^{-1}$ (**IV**) and $D_q$ = 1468$cm^{-1}$, $B$ = 515 $cm^{-1}$ (**V**). The $B$ parameter is approximately 67.5% (**IV**) and 59.8% (**V**) of that of the $V^{3+}$ free ion (861 $cm^{-1}$),[20] suggesting reasonable significant covalent character for the V–O/F bonds. The compound, $[C_2N_2H_{10}][(V^{IV}O)_3(H_2O)(HPO_3)_4]\cdot H_2O$ (**VI**)[15] contains an oxovanadium ($VO^{2+}$) group and exhibits three bands at 11037, 15313, and 22321 $cm^{-1}$. The large intensity of the charge-transfer band masks the latter (22321 $cm^{-1}$) band. These bands correspond to $^2E\rightarrow{}^2B_2$, $^2B_1\rightarrow{}^2B_2$, and $^2A_1\rightarrow{}^2B_2$ transitions and are generally referred to as bands I, II, and III, respectively.[21a,21b] Similar observations have been made for other compounds containing the $VO^{2+}$ species.[21c]

## Magnetic Properties

Magnetic susceptibility studies of compounds **II**–**V** and $[C_2N_2H_{10}][(V^{IV}O)_3(H_2O)(HPO_3)_4]\cdot H_2O$ (**VI**) were carried out on the powdered samples in the temperature range 300–2 K by using a SQUID magnetometer (MPMS, Quantum Design, USA).

The molar magnetic susceptibility of compounds **II**–**V** increases with decreasing temperature and reaches a maximum at low temperatures (Table S3, Supporting Information), indicating that long-range magnetic ordering is achieved. The observed effective magnetic moment ($\mu_{eff}$) at 300 K for the cobalt-containing compounds is 4.15 $\mu_B$ (in **II**) and 3.78 $\mu_B$ (in **III**), which is close to the expected spin-only value for the $Co^{2+}$ ions with spin $S$ = 3/2 (3.87 $\mu_B$) and in good agreement with the reported values.[22] A Curie–Weiss fit of the molar magnetic susceptibility at high temperatures (150–300 K) for **II** gave values of $C$ = 2.32 $cm^3$ K/mol and $\theta_p$ = –31.39 K (Figure 7a), and for **III** (150–300 K), $C$ = 1.91 $cm^3$ K/mol and $\theta_p$ = –19.18 K (Figure 7b). Structurally, compound **III** is made up of chains of edge-shared dimers of $Co^{2+}$ connected through the phosphite bridges, and a dimer model, based on the general isotropic exchange Hamiltonian, $\hat{H} = 2J\hat{S}_1\cdot\hat{S}_2$, 2, with $J$ = magnetic exchange coupling constant and $S_1 = S_2$ = 3/2 was employed to fit the observed magnetic data (Figure S6, Supporting Information). The susceptibility equation for the $Co^{2+}$ dimer can be obtained by substituting the values for the $Co^{2+}$ ion in a dimeric complex from the Van Vleck Equation (see Supporting Information).[23] Thus, the values of $N_A$ = Avogadro's number, $g$ = gyromagnetic ratio (ca. 2.0), $\mu_B$ = Bohr Magneton, $k$ = Boltzmann constant, $T$ = temperature, $J = J_{12} = J_{21}$ = the coupling constant between two neighboring metal centers, and $x = J/kT$ are included to give Equation (1).

$$\chi_M^{dimer} = \frac{N_A g^2 \mu_B^2 [14 + 5x^3 + x^5]}{kT[7 + 5x^3 + 3x^5 + x^6]} \quad (1)$$

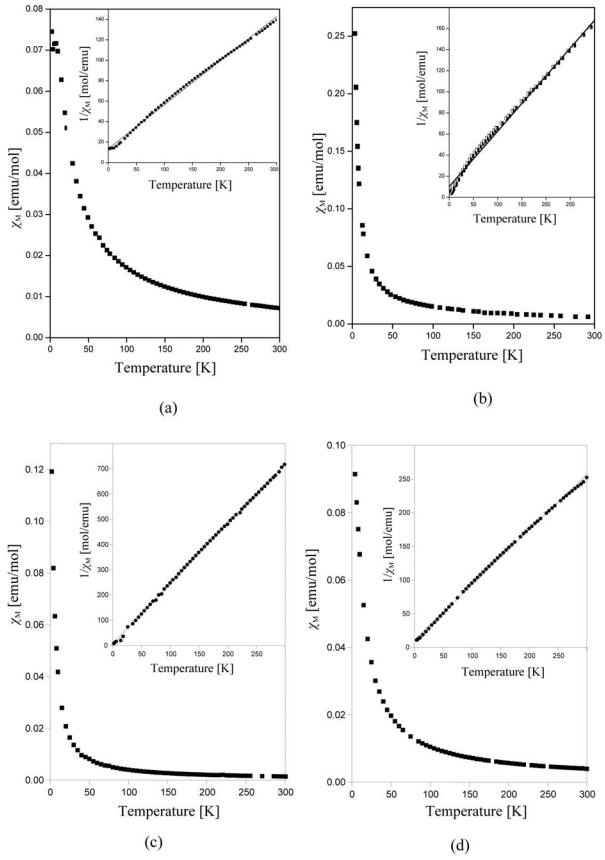


Figure 7. The $\chi_M$ vs. $T$ plots for (a) compound **II**, (b) compound **III**, (c) compound **IV**, and (d) compound **V**. Inset shows the $1/\chi_M$ vs. $T$ plot.

A good fit for the experimentally observed data was obtained with a $J$ value of –0.759 $cm^{-1}$. The small negative value for $J$ indicates weak antiferromagnetic interactions between the Co dimers in **III**. Similar values of $J$ have been observed previously in compounds containing dimeric dimeric cobalt species.[19a]

The vanadium phosphite compounds $[C_4N_2H_{14}][V^{III}F(HPO_3)_2]\cdot H_2O$ (**IV**) and $[C_3N_2H_5]_2[V_4^{III}(H_2O)_3(HPO_3)_4(HPO_4)_3]$ (**V**) also exhibited comparable magnetic behavior where the molar susceptibilities increase with decreasing temperature (Figure 7c,d). The high temperature data was fitted by using the Curie–Weiss equation in the range 100–300 K, with the values of $C$ = 0.42 $cm^3$ K/mol and $\theta_p$ = –2.81 K (compound **IV**), and $C$ = 1.22 $cm^3$ K/mol and $\theta_p$ = –13.25 K (compound **V**). At room temperature, the calcu-

  

lated $\mu_{eff}$ values are 2.42 and 3.09 $\mu_B$, respectively, and are in good agreement with the theoretical spin-only value for trivalent vanadium (2.83 $\mu_B$).

The magnetic susceptibility of compound $[C_2N_2H_{10}][(V^{IV}O)_3(H_2O)(HPO_3)_4]\cdot H_2O$[15] (**VI**) also exhibits similar behavior, where the molar magnetic susceptibility increases with decreasing temperature (Figure 8a). A Curie–Weiss fit of the high temperature data (60–300 K) gave values of $C$ = 1.59 $cm^3$ K/mol and $\theta_p$ = –11.61 K. The negative value of $\theta_p$ suggests that the interactions between the $V^{4+}$ ions, at high temperature, are antiferromagnetic. At room temperature, the observed magnetic moment ($\mu_{eff}$) is 2.06 $\mu_B$, which is close to the calculated spin-only value for $V^{4+}$ ($d^1$) (1.73 $\mu_B$). A plot of $\chi_M T$ vs. $T$ indicates that at low temperatures (<10 K), there is a sharp rise in the values of $\chi_M T$ (Figure 8b), suggesting a possible change in the interactions between the $V^{4+}$ ions. A study of the dependence of the magnetization as a function of different field strengths shows that the magnetization saturates at 5000 Oe (Figure 8c). The low magnetic field studies indicate a small hysteresis, with coercive field and remnant magnetization values of 17.7 Oe and 4.77 emu/mol, respectively. This suggests that there could be weak ferromagnetic interactions between the $V^{4+}$ ions at low temperatures in this compound.

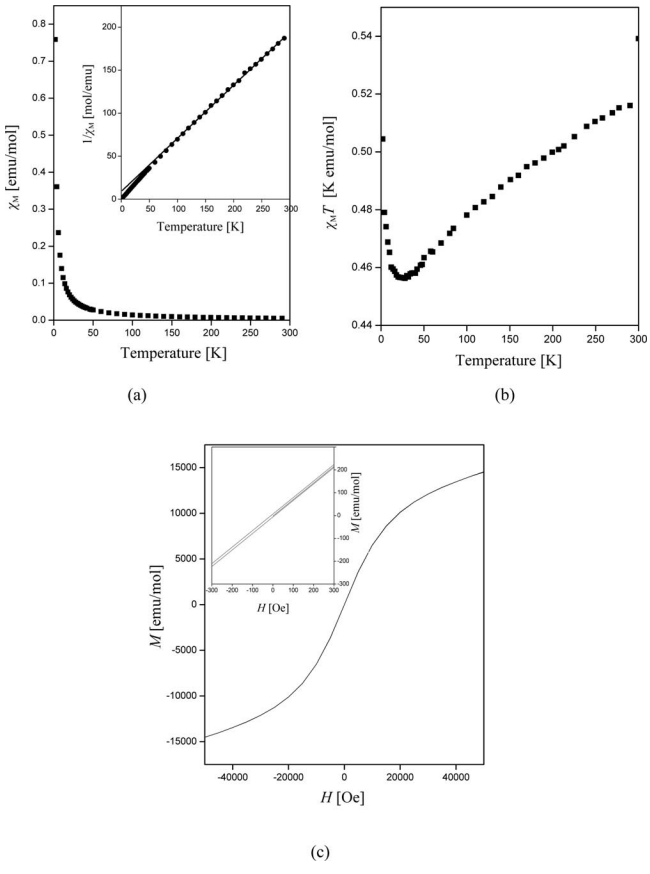


Figure 8. (a) The $\chi_M$ vs. $T$ plot for $[C_2N_2H_{10}][(V^{IV}O)_3(H_2O)(HPO_3)_4]\cdot H_2O$[15] (**VI**). Inset shows the $1/\chi_M$ vs. $T$ plot. (b) The $\chi_M T$ vs. $T$ plot for **VI**. (c) The $M$ vs. $H$ behavior of $[C_2N_2H_{10}][(V^{IV}O)_3(H_2O)(HPO_3)_4]\cdot H_2O$ (**VI**). The inset shows the behavior at low fields.

## ESR Studies

We have also employed ESR studies as a function of temperature to probe the interactions between the $V^{4+}$ centers in $[C_2N_2H_{10}][(V^{IV}O)_3(H_2O)(HPO_3)_4]\cdot H_2O$ (**VI**). The X-band ESR spectra were recorded on the powdered sample in the temperature range 3.8–300 K (Figure 9a). The calculated $g$ value of 1.966 indicates that the vanadium species are present in the +4 oxidation state in this compound. The spectra did not exhibit any appreciable change in the temperature range 300–100 K. The line width of the ESR signal, however, exhibits a small increase, which could be due to the dipolar homogeneous broadening (Figure 9b).[24] The line width starts to broaden below 100 K along with an increase in the peak-to-peak intensity, which reaches a

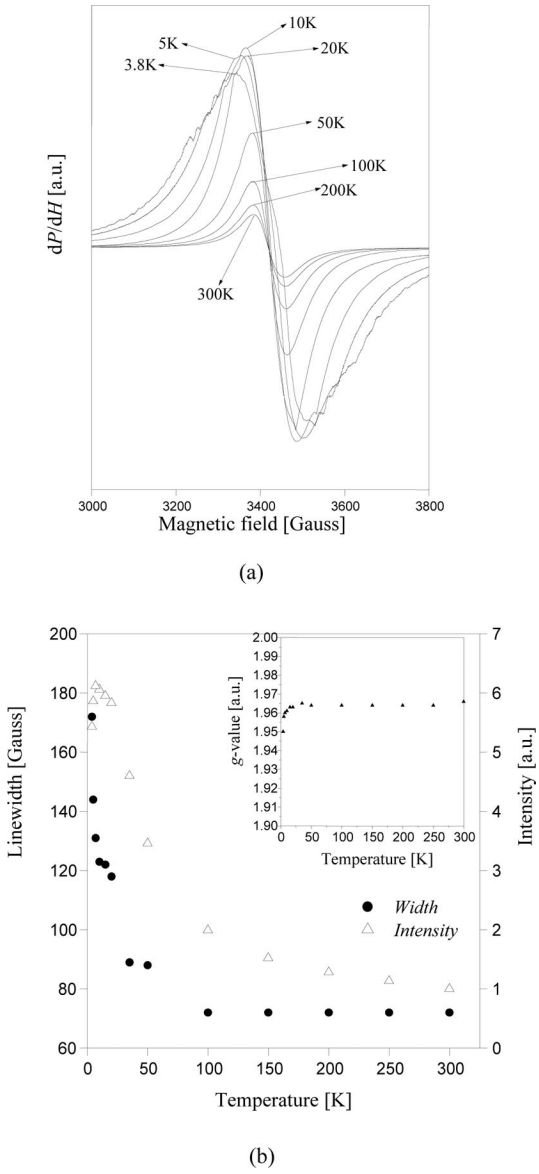


Figure 9. (a) The X-band ESR spectra of compound $[C_2N_2H_{10}][(V^{IV}O)_3(H_2O)(HPO_3)_4]\cdot H_2O$[15] (**VI**) at different temperatures. (b) Temperature dependence of the intensity and line width of the ESR signals. Inset shows the temperature dependence of the $g$-value.

  

maximum at around 7 K. This observation clearly indicates that at low temperatures, the magnetic centers interact strongly and the spins are strongly correlated. Thus, the ESR study appears to support the observation of weak ferromagnetic interactions at low temperatures in our magnetic studies. Similar behavior has been encountered in other related systems.[24,25]

## Experimental Section

**Synthesis:** Compounds **I** and **II** were synthesized by employing nonaqueous solvothermal conditions with the use of an organophosphorus source in place of $H_3PO_3$. The various synthesis conditions employed in the present study are listed in Table 3. For the synthesis of compound **I**, $CoCl_2{\cdot}6H_2O$ (0.245 g, 1 mmol) was mixed with 2-butanol (9.2 mL, 100 mmol). Triethylphosphite (TEP; 0.69 mL, 4 mmol) and piperazine (0.435 g, 5 mmol) were added, and the mixture was stirred until it became homogeneous. The final mixture with composition $1.0CoCl_2/6.0H_2O$/4.0TEP/5.0piperazine/100(2-butanol) was heated in a 23-mL autoclave at 180 °C for 48 h. The solid products in **I** and **II** consisted of deep-blue needle-like crystals. We observed that compound **I** started to turn pink upon exposure to air, and hence, other than the single-crystal structure, we have not been able to perform further characterizations. For the preparation of compound **III**, a reaction mixture of the composition $1.0Co(OH)_2/4.0H_3PO_3$/2.0(4,4′-bipyridine)/$200H_2O$ was heated at 110 °C for 7 d in a 7-mL PTFE-lined acid digestion bomb. In all the cases, reasonable yields of the products were obtained.

For the preparation of the vanadium phosphite phases, a similar hydrothermal synthetic method was employed, where both the source of the vanadium as well as the organic amine molecules were different for different phases (Table 3).

**Initial Characterizations:** The initial characterizations were carried out by using powder X-ray diffraction (XRD), thermogravimetric analysis (TGA), and infrared spectroscopy (IR) measurements. Elemental analysis of the compounds was carried out by using a CHNS analyzer (ThermoFinnigan FLASH EA 1112 CHNS analyzer). The results are presented in Table S4 (Supporting Information).

The powder XRD patterns were recorded on well-ground powdered samples in the $2\theta$ range 5–50° by using Cu-$K_\alpha$ radiation ($\lambda$ = 1.5405 Å) (Philips, X′pert Pro). The experimental XRD patterns are consistent with the simulated XRD patterns generated from the structures determined by using the single-crystal XRD, though the intensity of some of the peaks does not match. This could be due to the preferred orientation effects known in powder XRD experiments (see Figure S7, Supporting Information).

TGA (Mettler–Toledo, ThermoSTAR) studies were performed in an atmosphere of flowing air (flow rate = 50 mL/min) in the temperature range 25–700 °C (heating rate = 5 °C/min; see Figure S8, Supporting Information). The decomposition curve of $[C_4N_2H_{14}][Co(HPO_3)_2]$ (**II**) reveals a continuous mass loss (obsd. 21.20%) over a temperature range of 350–500 °C, which could be due to the decomposition of the amine molecule (calcd. 29.13%). The final decomposed product was found to be amorphous by powder XRD. For $[Co(C_{10}H_8N_2)\ (H_2PO_3)_2]$ (**III**), the result indicates a single sharp weight loss (obsd. 33.32%) over a broad temperature range of 200–500 °C, which is due to the loss of the amine molecules (calcd. 41.38%). The final decomposition product after the TGA studies was found to be crystalline by powder XRD ($Co_2P_4O_{12}$, JCPDS: 40-0068). The difference between the observed and the calculated weight losses in compounds **II** and **III** may be explained by taking into consideration the oxidation of $P^{III}$ to $P^{V}$, which corresponds to 10.36% (**II**) and 8.48% (**III**). The total weight loss, then, would be 31.56% (21.20 + 10.36) and 41.80% (33.32 + 8.48), which is considerably closer to the calculated weight loss of 29.13 and 41.38% for cobalt phosphite phases **II** and **III**, respectively. For the vanadium phosphite $[C_4N_2H_{14}][V^{III}F(HPO_3)_2]{\cdot}H_2O$ (**IV**), the weight loss of 29.40% appears to be a continuous one, which could be due to the loss of the amine molecules (calcd. 26.63%) and the loss of fluorine (calcd. 5.65%) and water molecules (calcd. 5.33%). For $[C_3N_2H_5]_2[V_4^{III}(H_2O)_3(HPO_3)_4(HPO_4)_3]$ (**V**), the weight loss occurs in two steps. The first small weight loss of 2.07% in the temperature range from room temperature to 250 °C (obsd. 2.07%) may be due to the partial loss of coordinated

Table 3. Summary of the synthesis conditions employed in the present study for compounds **I**–**VI**.

| Mole ratio | Temp [°C] | Time [h] | Yield [%] (Based on metal) | Product | Color |
|---|---|---|---|---|---|
| $1.0CoCl_2/6.0H_2O$/4.0TEP/5.0piperazine/100(2-butanol) | 180 | 48 | 40 | $[C_4N_2H_{12}][Co(HPO_3)_2]$, **I**[a] + powder | blue crystals + pink powder |
| $1.0CoCl_2{\cdot}6H_2O$/4.0TEP/4.0(1,4-DAB)/100(2-butanol) | 180 | 72 | 60 | $[C_4N_2H_{14}][Co(HPO_3)_2]$, **II** | blue |
| $1.0Co(OH)_2/4.0H_3PO_3$/2.0(4,4′-bipyridine)/$200H_2O$ | 110 | 168 | 85 | $[Co(C_{10}H_8N_2)\ (H_2PO_3)_2]$, **III** | pink |
| $1.0V_2O_5/10.0H_3PO_3$/5.0(1,4-DAB)/5.0HF/$233H_2O$ | 150+180 | 72+48 | 85 | $[C_4N_2H_{14}][V^{III}F(HPO_3)_2]{\cdot}H_2O$, **IV** | green |
| $1.0VOSO_4/5.0H_3PO_3$/2.0imidazole/$333H_2O$ | 150+180 | 48+48 | 80 | $[C_3N_2H_5]_2[V_4^{III}(H_2O)_3(HPO_3)_4(HPO_4)_3]$, **V** | green |
| $1.0V_2O_3$/3.0HCl/$3.0H_3PO_3/2.0H_2C_2O_4$/2.0ethylenediamine/$555H_2O$[b] | 165+200 | 72+24 | 75 | $[C_2N_2H_{10}][(V^{IV}O)_3(H_2O)(HPO_3)_4]{\cdot}H_2O$,[15] **VI** | blue |

[a] Unstable, changes color quickly (blue to pink). [b] The synthesis of $[C_2N_2H_{10}][(V^{IV}O)_3(H_2O)(HPO_3)_4]{\cdot}H_2O$ by Feng et al.[15] was carried out from a reaction mixture with the composition $1.0V_2O_5/10.0H_3PO_3$/9.0en/$232H_2O$ heated at 160 °C for 120 h.

  

Table 4. Crystal data and structure refinement parameters for compounds **I**–**V**.[a]

| | **I** | **II** | **III** | **IV** | **V** |
|---|---|---|---|---|---|
| Empirical formula | $C_4H_{14}CoN_2O_6P_2$ | $C_4H_{16}CoN_2O_6P_2$ | $C_{10}H_{12}CoN_2O_6P_2$ | $C_4H_{18}VFN_2O_7P_2$ | $C_6H_{23}N_4O_{27}P_7V_4$ |
| Formula weight | 307.04 | 309.06 | 377.09 | 337.94 | 1003.766 |
| Crystal system | monoclinic | monoclinic | monoclinic | orthorhombic | trigonal |
| Space group | *C*2/*c* (no.15) | *C*2/*c* (no.15) | *C*2/*c* (no.15) | *Imma* (no.74) | $P\bar{3}c1$ (no.165) |
| Crystal size [mm] | 0.16 × 0.08 × 0.06 | 0.16 × 0.08 × 0.06 | 0.16 × 0.14 × 0.08 | 0.24 × 0.10 × 0.08 | 0.20 × 0.12 × 0.08 |
| *a* [Å] | 17.774(5) | 17.661(10) | 17.2718(6) | 7.2125(11) | 13.4985(14) |
| *b* [Å] | 7.248(2) | 8.742(5) | 11.4561(4) | 9.2842(14) | 13.4985(14) |
| *c* [Å] | 8.813(3) | 8.056(5) | 16.9932(5) | 16.730(3) | 18.120(4) |
| *α* [°] | 90 | 90 | 90 | 90 | 90 |
| *β* [°] | 105.151(5) | 97.151(9) | 119.014(10) | 90 | 90 |
| *γ* [°] | 90 | 90 | 90 | 90 | 120 |
| Volume [Å$^3$] | 1095.9(5) | 1234.2(12) | 2940.42(17) | 1120.3(3) | 2280.35(6) |
| *Z* | 8 | 8 | 8 | 4 | 12 |
| Temperature [K] | 293 | 293 | 293 | 293 | 293 |
| $\rho_{calcd.}$ [g/cm$^3$] | 1.861 | 1.663 | 1.704 | 1.864 | 2.143 |
| *μ* [1/mm] | 1.868 | 1.659 | 1.411 | 1.206 | 1.765 |
| Wavelength [Å] | 0.71073 | 0.71073 | 0.71073 | 0.71073 | 0.71073 |
| *θ* range [°] | 2.37 to 28.06 | 2.32 to 28.04 | 2.23 to 23.29 | 2.43 to 26.36 | 1.74 to 28.01 |
| Reflection collected | 4547 | 4858 | 6037 | 3955 | 20659 |
| Unique reflections | 1291 | 1400 | 2119 | 591 | 2091 |
| Number of parameters | 69 | 69 | 191 | 55 | 148 |
| Goodness of fit | 1.150 | 1.079 | 1.083 | 1.122 | 1.065 |
| R index [$I > 2\sigma(I)$] | $R_1$ = 0.0485<br>$wR_2$ = 0.1315 | $R_1$ = 0.0553<br>$wR_2$ = 0.1276 | $R_1$ = 0.0423<br>$wR_2$ = 0.1189 | $R_1$ = 0.0881<br>$wR_2$ = 0.2330 | $R_1$ = 0.0499<br>$wR_2$ = 0.1317 |

[a] $R_1 = \Sigma||F_o| - |F_c||/\Sigma|F_o|$; $wR_2 = \{\Sigma[w(F_o^2 - F_c^2)]/\Sigma[w(F_o^2)^2]\}^{1/2}$. $w = 1/[\rho^2(F_o)^2 + (aP)^2 + bP]$. $P = [\max(F_o, O) + 2(F_c)^2]/3$, where $a$ = 0.0643 and $b$ = 5.3209 for **I**, $a$ = 0.0632 and $b$ = 3.7048 for **II**, $a$ = 0.0580 and $b$ = 7.1718 for **III**, $a$ = 0.1372 and $b$ = 15.6808 for **IV**, $a$ = 0.0779 and $b$ = 11.2585 for **V**.

water molecules (calcd. 5.36%). The second broad weight loss of 10.14% in the range 250–700 °C corresponds to the loss of all the water molecules as well as the amine molecules (calcd. 15.76%). Again, the difference in the observed and calculated weight losses can be accommodated by considering the oxidation of $P^{III}$ to $P^{V}$ during the TGA studies [9.47% (**IV**) and 6.23% (**V**)]. The total weight loss of 35.62% (29.39 + 9.47) and 18.44% (12.21 + 6.23) is considerably closer to the expected weight loss of 37.61% in **IV** and 21.01% in **V**. The calcined products in both **IV** and **V** were found to be amorphous by powder XRD.

IR spectroscopic studies were carried out in the mid-IR range 400–4000 cm$^{-1}$ by using the KBr pellet method (Perkin–Elmer, SPECTRUM 1000; see Figure S9 and Table S5, Supporting Information).

**Single-Crystal Structure Determination:** A suitable single crystal of each compound was carefully selected and glued to a thin glass fiber. The single-crystal diffraction data were collected with a Bruker AXS Smart Apex CCD diffractometer at room temperature (293 K). The X-ray generator was operated at 50 kV and 35 mA by using Mo-$K_\alpha$ ($\lambda$ = 0.71073 Å) radiation. Data were collected with $\omega$ scans of width 0.3°. A total of 606 frames were collected in three different settings of $\phi$ (0, 90, and 180°) by keeping the sample-to-detector distance fixed at 6 cm and the detector position fixed at –25°. Pertinent experimental details of the structure determination are listed in Table 4.

The data were reduced by using SAINTPLUS[26] and an empirical absorption correction was applied by using the SADABS program.[27] The crystal structure was solved and refined by direct methods with the use of SHELXL-97 present in the WinGx suite of programs.[28] The organic amine molecules in **IV** could not be located and appear to be fragmented. The lattice water molecule in **IV** and the amine molecules in **V** were found to be disordered, and hence, the hydrogen atoms could not be located in the Fourier map. The hydrogen position for the P–H group for compounds **I**–**III** and **V**, and the hydrogen positions of the water molecules and amine molecules of compounds **I**–**III**, could be identified from the difference Fourier maps. For the final refinement the hydrogen atoms were placed in geometrically ideal positions and refined by using the riding mode. Bond valence calculations[11b] for the P(1) atom in compound **IV** gave a value of 4.009, corresponding to the presence of the $HP^{4+}$ group. The presence of the $HPO_3^{2-}$ anion was also confirmed by IR spectroscopy, which gave a band at 2420 cm$^{-1}$ [ν(HP)]. The last cycles of refinement for compounds **I**–**V** included all the atomic positions and anisotropic thermal parameters for all the non-hydrogen atoms and the isotropic thermal parameters for all the hydrogen atoms. Full-matrix-least-squares structure refinement against $|F|^2$ was carried out by using the WinGx suite of programs.[28] CCDC-757778 (for **I**), -757779 (for **II**), -297879 (for **III**), -757780 (for **IV**), and -757781 (for **V**) contain the supplementary crystallographic data for this paper. These data can be obtained free of charge from The Cambridge Crystallographic Data Centre via www.ccdc.cam.ac.uk/data_request/cif.

**Supporting Information** (see footnote on the first page of this article): Selected bond angles and distances, magnetic parameters for the compounds, details of the elemental analyses, crystal data and structure refinement parameters for compound **VI**, figures showing the structure of compound **VI**, IR spectra, simulated and experimental XRD patterns of compounds, TGA curves, details of the magnetic modeling.

## Acknowledgments

S.N. thanks the Department of Science and Technology (DST), Government of India and the Council of Scientific and Industrial Research (CSIR), Government of India for the award of a research grant. S.N. also thanks the DST for the award of a RAMANNA

  

fellowship. The authors thank Ms. Oindrila Sengupta for her assistance with the modeling of the magnetic behavior.

[1] S. Natarajan, S. Mandal, *Angew. Chem. Int. Ed.* **2008**, *47*, 4798–4828.
[2] D. Maspoch, D. Ruiz-Molina, J. Veciana, *Chem. Soc. Rev.* **2007**, *36*, 770–818.
[3] A. K. Cheetham, T. Loiseau, G. Ferey, *Angew. Chem. Int. Ed.* **1999**, *38*, 3268–3292.
[4] S. T. Wilson, B. M. Lok, C. A. Messina, T. R. Cannan, E. M. Flanigen, *J. Am. Chem. Soc.* **1982**, *104*, 1146–1147.
[5] T. Rojo, J. L. Mesa, J. Lago, B. Bazan, J. L. Pizarro, M. I. Arriortua, *J. Mater. Chem.* **2009**, *19*, 3793–3818.
[6] a) J. Fan, C. Slebodnick, B. E. Hanson, *Inorg. Chem. Commun.* **2006**, *9*, 103–106; b) Z.-E. Lin, W. Fan, J. Gu, T. Okubo, *J. Solid State Chem.* **2007**, *180*, 981–987; c) W. T. A. Harrison, R. M. Yeates, M. L. F. Philips, T. M. Nenoff, *Inorg. Chem.* **2003**, *42*, 1493–1498; d) S. Mandal, S. Natarajan, *Solid State Sci.* **2006**, *8*, 388–396; e) L. Hu, J. Fan, C. Slebodnick, B. E. Hanson, *Inorg. Chem.* **2006**, *45*, 7681–7688; f) D. Zhang, H. Yue, Z. Shi, S. Feng, *Solid State Sci.* **2005**, *7*, 1256–1260.
[7] a) G. Bonavia, J. DeBord, R. C. Haushalter, D. Rose, J. Zubieta, *Chem. Mater.* **1995**, *7*, 1995–1998; b) Z. Shi, D. Zhang, G. Li, L. Wang, X. Li, J. Hua, S. Feng, *J. Solid State Chem.* **2003**, *172*, 464–470; c) S. Fernandez, J. L. Mesa, J. L. Pizarro, L. Lezama, M. I. Arriortua, T. Rojo, *Angew. Chem. Int. Ed.* **2002**, *41*, 3683–3685; d) S. Fernandez, J. L. Mesa, J. L. Pizarro, L. Lezama, M. I. Arriortua, R. Olazcuaga, T. Rojo, *Chem. Mater.* **2000**, *12*, 2092–2098; e) U.-C. Chung, J. L. Mesa, J. L. Pizarro, J. R. Fernandez, J. S. Marcos, J. S. Garitaonandia, M. I. Arriortua, T. Rojo, *Inorg. Chem.* **2006**, *45*, 8965–8972; f) S. F. Armas, J. L. Mesa, J. L. Pizarro, U.-C. Chung, M. I. Arriortua, T. Rojo, *J. Solid State Chem.* **2005**, *178*, 3554–3562.
[8] W. T. A. Harrison, *Solid State Sci.* **2003**, *5*, 297–302.
[9] S. Fernandez, J. L. Pizarro, J. L. Mesa, L. Lezama, M. I. Arriortua, T. Rojo, *Int. J. Inorg. Mater.* **2001**, *3*,331–336.
[10] a) S. Mandal, S. K. Pati, M. A. Green, S. Natarajan, *Chem. Mater.* **2005**, *17*, 638–643; b) S. Mandal, D. Banerjee, S. V. Bhat, S. K. Pati, S. Natarajan, *Eur. J. Inorg. Chem.* **2008**, 1386–1391.
[11] a) I. D. Brown, D. Altermatt, *Acta Crystallogr., Sect. B* **1985**, *41*, 244–247; b) J. Loub, *Acta Crystallogr., Sect. B* **1991**, *47*, 468–473.
[12] F. C. Hawthrone, *Acta Crystallogr., Sect. B* **1994**, *50*, 481 and the references cited therein.
[13] a) J. M. Thomas, R. H. Jones, R. Xu, J. Chen, A. M. Chippindale, S. Natarajan, A. K. Cheetham, *J. Chem. Soc., Chem. Commun.* **1992**, 929–931; b) P. A. Barrett, R. H. Jones, *J. Chem. Soc., Chem. Commun.* **1995**, 1979–1981; c) S. Oliver, A. Kuperman, A. Lough, G. A. Ozin, *Inorg. Chem.* **1996**, *35*, 6373–6380; d) A. M. Chippindale, A. R. Cowley, Q. Huo, R. H. Jones, A. D. Law, J. M. Thomas, R. Xu, *J. Chem. Soc., Dalton Trans.* **1997**, 2639–2644.
[14] a) C. Chen, Y. Liu, Q. Fang, L. Liu, J. F. Eubank, N. Zhang, S. Gong, W. Pang, *Microporous Mesoporous Mater.* **2006**, *97*, 132–140; b) S. Shi, L. Wang, H. Yuan, G. Li, J. Xu, G. Zhu, T. Song, S. Qiu, *J. Solid State Chem.* **2004**, *177*,4183–4187.
[15] D. Zhang, H. Yue, Z. Shi, M. Guo, S. Feng, *Microporous Mesoporous Mater.* **2005**, *82*, 209–213.
[16] a) S. Neeraj, C. N. R. Rao, A. K. Cheetham, *J. Mater. Chem.* **2004**, *14*, 814–820; b) S. Neeraj, M. L. Noy, C. N. R. Rao, A. K. Cheetham, *J. Solid State Chem.* **2002**, *167*, 344–353; c) S. Neeraj, M. L. Noy, A. K. Cheetham, *Solid State Sci.* **2002**, *4*, 397–404.
[17] A. Choudhury, S. Natarajan, C. N. R. Rao, *J. Chem. Soc., Dalton Trans.* **2000**, 2595–2598.
[18] R. A. Ramik, B. D. Sturman, P. J. Dunn, A. S. Povarennykh, *Can. Mineral.* **1980**, *18*, 185–190.
[19] a) A. Dakhlaoui, S. Ammar, L. S. Smiri, *Mater. Res. Bull.* **2005**, *40*, 1270–1278; b) C. Chen, Y. Liu, S. Wang, G. Li, M. Bi, Z. Yi, W. Pang, *Chem. Mater.* **2006**, *18*, 2950–2958; c) R.-Q. Fan, D.-S. Zhu, Y. Mu, G.-H. Li, Y.-L. Yang, Q. Su, S.-H. Feng, *Eur. J. Inorg. Chem.* **2004**, 4891–4897.
[20] A. B. P. Lever, *Inorganic Electronic Spectroscopy*, Elsevier Science Publishers, Amsterdam, Netherlands, **1984**.
[21] a) J. Selbin, *Chem. Rev.* **1965**, *65*, 153–175; b) C. J. Ballhausen, H. B. Gray, *Inorg. Chem.* **1962**, *1*, 111–122; c) T. Berrocal, J. L. Mesa, J. L. Pizarro, B. Bazán, M. Iglesias, J. L. Vilas, T. Rojo, M. I. Arriortua, *Dalton Trans.* **2010**, *39*, 834–846.
[22] a) P. Cossee, A. E. Van Arkel, *J. Phys. Chem. Solids* **1960**, *15*, 1–6; b) S. Mandal, S. Natarajan, *J. Solid State Chem.* **2005**, *178*, 2376–2382.
[23] O. Kahn, *Molecular Magnetism*, VCH Publishers, Weinheim, **1993**.
[24] a) H. W. Wijn, L. R. Walker, J. L. Daris, H. J. Guggenheim, *Solid State Commun.* **1972**, *11*, 803–805; b) A. Escuer, R. Vicente, M. A. S. Goher, F. Mautner, *Inorg. Chem.* **1995**, *34*,5707–5708; c) T. T. P. Cheung, Z. G. Soos, R. E. Dietz, F. R. Merrit, *Phys. Rev. B* **1978**, *17*, 1266–1276.
[25] A. Bensini, D. Gatteschi, *EPR of Exchange Coupled Systems*, Springer, Berlin, **1990**.
[26] SMART (v5.628), SAINT (v6.45a), XPREP, *SHELXTL*, Bruker AXS Inc. Madison, Wisconsin, USA, **2004**.
[27] G. M. Sheldrick, *Siemens Area Correction Absorption Correction Program*, University of Göttingen, Göttingen, Germany, **1994**.
[28] G. M. Sheldrick, *SHELXL-97, Program for Crystal Structure Solution and Refinement*, University of Göttingen, Göttingen, Germany, **1997**.

Received: December 14, 2009
Published Online: March 18, 2010

  